


RESEARCH ARTICLE

Tumor Markers and Signatures

Three-dimensional nuclear architecture distinguishes thyroid cancer histotypes

Aline Rangel-Pozzo¹ | Filipe F. dos Santos^{2,3} | Tinuccia Dettori⁴ |
 Matteo Giulietti⁵ | Daniela Virginia Frau⁴ | Pedro A. F. Galante² |
 Roberta Vanni⁶ | Alok Pathak⁷ | Gabor Fischer⁸ | John Gartner⁸ |
 Paola Caria⁴ | Sabine Mai¹ 

¹CancerCare Manitoba Research Institute, CancerCare Manitoba, University of Manitoba, Winnipeg, Canada

²Centro de Oncologia Molecular, Hospital Sirio-Libanes, Sao Paulo, Brazil

³Department of Biochemistry, Chemistry Institute, Universidade de Sao Paulo, Sao Paulo, Brazil

⁴Department of Biomedical Sciences, University of Cagliari, Monserrato, Italy

⁵Department of Specialistic Clinical and Odontostomatological Sciences, Polytechnic University of Marche, Ancona, Italy

⁶University of Cagliari, Department of Biomedical Sciences, University of Cagliari, Monserrato, Italy

⁷Department of Surgery, University of Manitoba, Winnipeg, Canada

⁸Department of Pathology, Max Rady College of Medicine, Rady Faculty of Health Sciences, University of Manitoba, Winnipeg, Canada

Correspondence

Paola Caria, Department of Biomedical Sciences, University of Cagliari, Monserrato, Italy.
 Email: paola.caria@unica.it

Sabine Mai, CancerCare Manitoba Research Institute, CancerCare Manitoba, University of Manitoba, Winnipeg, Canada.
 Email: sabine.mai@umanitoba.ca

Abstract

Molecular markers can serve as diagnostic tools to support pathological analysis in thyroid neoplasms. However, because the same markers can be observed in some benign thyroid lesions, additional approaches are necessary to differentiate thyroid tumor subtypes, prevent overtreatment and tailor specific clinical management. This applies particularly to the recently described variant of thyroid cancer referred to as noninvasive follicular thyroid neoplasm with papillary-like nuclear features (NIFTP). This variant has an estimated prevalence of 4.4% to 9.1% of all papillary thyroid carcinomas worldwide. We studied 60 thyroid lesions: 20 classical papillary thyroid carcinoma (CPTC), 20 follicular variant of PTC (FVPTC) and 20 NIFTP. We examined morphological and molecular features to identify parameters that can differentiate NIFTP from the other PTC subtypes. When blindly investigating the nuclear architecture of thyroid neoplasms, we observed that NIFTP has significantly longer telomeres than CPTC and FVPTC. Super-resolved 3D-structured illumination microscopy demonstrated that NIFTP is heterogeneous and that its nuclei contain more densely packed DNA and smaller interchromatin spaces than CPTC and FVPTC, a pattern that resembles normal thyroid tissue. These data are consistent with the observed indolent biological behavior and favorable prognosis associated with NIFTP, which lacks *BRAF*^{V600E} mutations. Of note, next-generation thyroid oncopanel sequencing was unable to distinguish the thyroid cancer histotypes in our study cohort. In summary, our data suggest that 3D

Abbreviations: 3D, three-dimensional; 3D-SIM, three-dimensional structured illumination microscopy; *BRAF*, v-raf murine sarcoma viral oncogene homolog B1; CPTC, classical papillary thyroid carcinoma; DAPI, 4',6-diamidino-2-phenylindole; FFPE, formalin-fixed paraffin-embedded; FVPTC, follicular variant of PTC; LN, lymph nodes; NAT, normal adjacent thyroid tissue; NIFTP, noninvasive follicular thyroid neoplasm with papillary-like nuclear features; *PPAR*_γ, peroxisome proliferator-activated receptor gamma; PTC, papillary thyroid carcinoma; Q-FISH, quantitative fluorescence in situ hybridization; *RAS*, rat sarcoma virus; *RET*, rearranged during transfection; *THADA*, thyroid adenoma-associated.

This is an open access article under the terms of the [Creative Commons Attribution-NonCommercial-NoDerivs](https://creativecommons.org/licenses/by-nc-nd/4.0/) License, which permits use and distribution in any medium, provided the original work is properly cited, the use is non-commercial and no modifications or adaptations are made.

© 2023 The Authors. *International Journal of Cancer* published by John Wiley & Sons Ltd on behalf of UICC.

Funding information

Rady Innovation Fund, Grant/Award Number: 50497

nuclear architecture can be a powerful analytical tool to diagnose and guide clinical management of NIFTP.

KEYWORDS

3D-SIM, histotypes differentiation, papillary thyroid carcinoma, targeted sequencing, telomeres molecular profile

What's new?

To improve diagnosis and management of thyroid cancer, greater knowledge of the molecular profiles that characterize different variants of thyroid malignancy is needed. Here, the authors identified and compared molecular features of noninvasive follicular thyroid neoplasm with papillary-like nuclear features (NIFTP), classical papillary thyroid carcinoma (CPTC) and follicular variant of PTC (FVPTC). Thyroid cancer histotypes were clearly differentiated by three-dimensional (3D) telomere profiling and 3D-structured illumination microscopy. Compared to CPTC and FVPTC, NIFTP exhibited a higher frequency of long telomeres, more densely packed DNA, and smaller interchromatin spaces. By contrast, next generation thyroid oncopanel sequencing was unable to make this distinction.

1 | INTRODUCTION

Over the past 30 years, the incidence of thyroid cancer has been steadily increasing in many other developed countries.¹ In most patients, the cause of thyroid cancer is unknown. Intensified surveillance has resulted in the detection of an increasing number of early thyroid cancers, especially papillary thyroid carcinoma (PTC). Despite its name, a papillary architecture is not required for diagnosis of PTC, which is defined by the presence of distinctive nuclear features.² The follicular variant of papillary thyroid carcinoma (FVPTC) is the most common variant of PTC.³ It is composed of neoplastic follicles rather than papillae, but the cancer cells have nuclear features similar to those of PTC. Previously, most patients with FVPTC regardless of the subtype (unencapsulated and encapsulated FVPTC) were treated as PTC. Due to over-diagnosis and over-treatment, encapsulated FVPTC without signs of invasion has since been reclassified and renamed “non-invasive follicular thyroid neoplasm with papillary-like nuclear features (NIFTP).”⁴ The name “NIFTP” appropriately reflects the biological characteristics and clinical behavior of this subtype, which includes a follicular growth pattern, presence of nuclei morphologically similar to those of PTC and lack of capsular invasion. The recognition of this new entity, initially based on histopathological criteria, was refined in 2018 with the introduction of primary and secondary criteria, including the absence of true papillae among the primary criteria and the absence of *BRAF*^{V600E} mutation or high-risk mutations among the secondary. The diagnosis of NIFTP requires primary criteria, but the secondary ones are helpful in the diagnosis but not required.

Our knowledge of the molecular profile of NIFTP is still evolving.⁵ The most recent literature indicates that NIFTP belongs to the RAS-like thyroid tumors and shows a high prevalence of RAS mutations, as well as other mutations normally associated with follicular thyroid tumors, such as *PPARγ*, *THADA* gene fusions with the absence of *BRAF*^{V600E}.⁶ Moreover, the presence of high-risk mutations such as

TERT promoter, *TP53* mutations and *ETV6-NTRK3* fusions are criteria that exclude the diagnosis of NIFTP.⁷ These molecular characteristics indicate that most NIFTP lesions are driven by clonal genetic alterations and indicate that they are true neoplasms and not hyperplastic proliferations. NIFTP lesions are considered as low risk for disease progression; however, several studies have demonstrated that among nodules diagnosed as NIFTP, there are some that give rise to metastatic disease, further emphasizing that lesions diagnosed as NIFTP do not always behave benignly.⁶ It is, therefore, evident that stringent histopathological criteria alone are insufficient to predict the behavior of these lesions and that additional approaches are needed. These tools could be an adjunct to the existing criteria used to identify NIFTP, and potentially help to predict the outcome of a given case and determine whether additional therapeutic measures should be instituted at the time of diagnosis.⁸

The genome of a normal cell is structurally different from that of a tumor cell. Recent quantitative measurements of the three-dimensional (3D) genome structure of normal vs tumor cell nuclei have indicated that these differences lie in how the genome is organized. Using centromeres, telomeres, chromosomes and DNA as tools to survey the 3D landscape, distinct changes can be identified and quantitated.⁹ These studies have shown that the genome structure can serve as architectural biomarker of cancer stage and aggressiveness.^{10,11} The 3D telomere organization in nuclei of cancer cells has enabled the distinction of stable or progressive disease in myelodysplastic syndromes and acute myeloid leukemia,¹¹ time to progression in glioblastoma,¹² response to treatment in Hodgkin lymphoma,¹³ stratification of patients into subgroups of disease aggressiveness in neuroblastoma,¹⁴ risk to progression in intermediate risk prostate cancer¹⁵ and risk to progression in multiple myeloma.¹⁶ Three-dimensional structured illumination microscopy (3D-SIM) imaging has enabled a closer look at the DNA structure in the nuclei of both normal and tumor cells. Our group was the first to describe quantitative measurements of DNA structure

(DNA organization in the interphase nuclei in nanoscale) using 3D-SIM in normal and Hodgkin lymphoma cells, multiple myeloma and in neuroblastoma.¹⁷⁻²⁰ A common observed feature was that DNA structure and DNA-poor interchromatin spaces differed between normal and tumor cells, as well as between normal, tumor cell precursors and tumor cells, with more interchromatin space in tumors than in normal cells.

In our study, we examined the spatial three-dimensional (3D) genome organization of NIFTP, classical PTC and FVPTC. We studied the 3D genome organization using telomeres as indicators for chromosome positions. We explored the overall DNA organization using 3D-SIM and quantitative analysis of the super-resolved DNA structure. In addition, we employed mutational targeted sequencing with a cancer oncopanel²¹ and performed fluorescence in situ hybridization and pathological analysis in 60 retrospective samples. We report that NIFTP was best distinguished from FVPTC and CPTC by the 3D nuclear architecture. Furthermore, NIFTP's nuclear architecture more closely resembled normal adjacent thyroid tissue (NAT) than CPTC and FVPTC. These findings were consistent with the less aggressive and heterogenous nature of NIFTP.

2 | MATERIALS AND METHODS

2.1 | Patient cohort

Retrospective cases diagnosed as CPTC, FVPTC and NIFTP were retrieved from the archives of the Anatomical Pathology Section of Max Rady College of Medicine (University of Manitoba, Winnipeg, Canada) for the interval 2018 to 2020 and new formalin-fixed paraffin-embedded (FFPE) sections (5 μ m) were prepared sequentially cut. Each case was reevaluated on hematoxylin and eosin-stained slides by two pathologists (JG and GF), according to the World Health Organization classification.²² The identified tumor area and the morphologically normal adjacent tissue area (NAT; at least 1 cm away from the tumor), were circled with a pen, to make it possible to recognize them in the unstained sections prepared in sequence for 3D and molecular analysis. In total, we analyzed 60 lesions: 20 CPTC (classic thyroid papillary carcinoma), 20 FVPTC and 20 NIFTP. For all PTC cases the following clinico-pathological characteristics were recorded: tumor size, presence of extrathyroidal extension, lymphovascular invasion, multifocality and American Joint Committee on Cancer T, N and M stages. All experiments were performed blinded for the tumor characteristics and patient outcome. Our cohort was composed of 11 (18.3%) men and 49 (81.6%) women, ages 23 to 78 (mean age of 50.6 years). Clinical and pathological characteristics of the 60 patients included in the study are shown in Table 1.

2.2 | Three-dimensional nuclear telomere analysis

Thyroid tissue samples were analyzed by 3D imaging using an AxioImager Z1 (Zeiss) following 3D quantitative FISH (Q-FISH). Forty

TABLE 1 Clinical information of the 60 patients examined in our study.

Parameter	
Age (mean)	50.6 years
Sex	
Male	11 (18.3%)
Female	49 (81.6%)
CPTC	20
Tumor size	
0-4 cm	18
\geq 4 cm	2
Focality	
Multifocal	10
Unifocal	10
Stage	
pT1a	5
pT1b	7
pT2	6
pT3	2
LN	6
FVPTC	20
Tumor size	
0-4 cm	16
\geq 4 cm	4
Focality	
Multifocal	8
Unifocal	12
Stage	
pT1a	7
pT1b	4
pT2	5
pT3	4
LN	1
NIFTP	20
Tumor size	
0-4 cm	18
\geq 4 cm	2
Focality	
Multifocal	6
Unifocal	14

Abbreviations: CPTC, classic thyroid papillary carcinoma; FVPTC, follicular variant PTC; LN, lymph nodes; NIFTP, noninvasive follicular thyroid neoplasm with papillary-like nuclear features.

z stacks were acquired using x, y: 102 nm and z: 200 nm. Telomeres were labeled with a Cy3-tagged peptide nucleic acid telomere probe (DAKO), and nuclei were counterstained using 4',6-diamidino-2-phenylindole (DAPI). Image stacks were analyzed following constrained iterative deconvolution, and all 3D telomere parameters were

measured using the TeloView program²³ (Telo Genomics Corp., Toronto, ON, Canada). One hundred nuclei (100) per sample were examined. TeloView determined the following six telomere parameters: telomere signal intensity (total and average), number of telomere signals, number of telomere aggregates (ie, clusters of telomeres too close to be further resolved at an optical resolution limit of 200 nm), nuclear volume, *a/c* ratio (ie, spatial distribution of the telomeres within the nucleus in a cell cycle-dependent manner) and distribution of telomeres relative to the nuclear periphery.

2.3 | Telomere statistical analysis

The software package SAS (SAS Institute Inc., Cary, NC, v9.4) was employed to perform nested factorial analysis of variance in the telomere parameters measured using TeloView. Chi-square tests were used to compare the percentage of interphase telomere signals at each given intensity level at intervals of 1000 intensity units, ultimately divided into quartiles for analysis. Nested factorial analysis of variance was also used to compare the distribution of signal intensities across NIFTP, FVTPC and CPTC. We considered statistical significance when the probability of type I error (alpha) was $\leq 5\%$ (P -value ≤ 0.05).

2.4 | Super-resolution imaging of nuclear DNA

Formalin-fixed and paraffin-embedded patient thyroid sections (5 μm -thick) were treated with xylene (2×15 min, Sigma-Aldrich) and tissues were rehydrated through incubation in solutions of descending concentration of ethanol: 100%, 90% and 70%, 5 min each. Subsequently, sections were incubated for 5 min in PBS and permeabilized using 0.75% TX-100 in PBS for 30 min at 37°C. Nuclear DNA was stained by overnight incubation with 50 $\mu\text{g}/\text{mL}$ DAPI followed by 1 min wash in PBS. A total of 100 cells (50 cells from tumor and 50 cells from NAT) for each sample were imaged with a Zeiss Elyra PS1 SIM equipped with a Plan Apochromat $\times 63/1.40$ Oil immersion objective using an ANDOR iXon DU 885 CCD camera and a $\times 1.6$ tube lens. The 3D-SIM images were reconstructed with ZEN 2012 black edition (Carl Zeiss, Jena, Germany) with the standard settings. The image processing and measurement steps were performed in Matlab (MathWorks, Natick, MA) with the toolbox DIP image.¹⁸ The granulometry program which analyzes the DNA structure and DNA-free space was used to measure the morphological sieve applied to the error-function clipped images¹⁸ and the two-sided, two-sample Kolmogorov-Smirnov (KS) tests are used to determine the significance between the differences observed.

2.5 | Genetic profile and analysis of thyroid-cancer associated genetic changes

DNA extraction was performed from 30 μm FFPE sections using the QIAamp DNA FFPE Tissue Kit (QIAGEN, Gaithersburg, MD)

according to the manufacturer's instructions. DNA concentration was assessed using Qubit dsDNA Assay kit on the Qubit 2.0 Fluorometer (Thermo Fisher Scientific, Waltham, MA). Targeted next-generation sequencing was performed on libraries prepared with the TruSeq Amplicon Cancer Panel (TSACP, Illumina) on the MiSeq sequencer (Illumina, San Diego, CA) to cover hotspot regions of 48 genes: *ABL1*, *AKT1*, *ALK*, *APC*, *ATM*, *BRAF*, *CDH1*, *CDKN2A*, *CSF1R*, *CTNNB1*, *EGFR*, *ERBB2*, *ERBB4*, *FBXW7*, *FGFR1*, *FGFR2*, *FGFR3*, *FLT3*, *GNA11*, *GNAQ*, *GNAS*, *GNF1A*, *HRAS*, *IDH1*, *JAK2*, *JAK3*, *KDR*, *KIT*, *KRAS*, *MET*, *MLH1*, *MPL*, *NOTCH1*, *NPM1*, *NRAS*, *PDGFRA*, *PIK3CA*, *PTEN*, *PTPN11*, *RB1*, *RET*, *SMAD4*, *SMARCB1*, *SMO*, *SRC*, *STK11*, *TP53* and *VHL*.²⁴ To generate a consistent set of somatic mutations, we used two different established pipelines for variant calling and additional quality control pipelines, as follows. First, we used FASTQC²⁵ and TRIMMOMATIC²⁶ to filter out adapters or low quality reads. Secondly, due to DNA quality, 12 tumor-normal pairs were excluded from further steps. Next, we used the Burrows-Wheeler Alignment tool (BWA-MEM), specifically the maximal exact matches algorithm²⁷ to align sequences from tumors and their normal adjacent tissue to human reference build (GRCh38/hg38). Somatic mutations were identified in the aligned data using BCFTOOLS CALL²⁸ and Genome Analysis Toolkit²⁹ (GATK—v4.1.4.0). In the GATK front, we performed the marking of duplicates (Mark Duplicates—v1.114), base recalibration (Picard Toolkit 2019; all parameters default) and variant calling with the “Haplotype Caller” tool²⁹ (all parameters default). Finally, we used ANNOVAR³⁰ for the annotation of variants. In addition, SAMTOOLS (v1.13) was used in many steps, such as sorting, indexing, filtering and getting a number of basic statistics like coverage.²⁸ Scripts in shell (Linux CentOS v8.5.2111), R (v4.1.0) (R Core Team) and Python (v3.6.15) were utilized in order to create and organize the entire pipeline.³¹

2.6 | RET and PPAR γ rearrangements

Double-target FISH probes containing DNA sequences flanking the breakpoints of the *RET* and *PPAR γ* genes (involved in *RET/PTC* and *PAX8* [or *CREB3L2*]/*PPAR γ* gene fusions) were used to identify *RET* and *PPAR γ* rearrangements. The analytical specificity (percentage of FISH signal located at the correct metaphase chromosome position of *RET* and *PPAR γ* genes) and sensitivity (percentage of metaphases or nuclei with FISH signal pattern), and a cutoff value of the break-apart *RET* and *PPAR γ* probes were previously demonstrated.³² Briefly, 100% specificity for both *RET* and *PPAR γ* and 99.5% sensitivity for *RET* and 99.8% for *PPAR γ* were established in metaphases and nuclei of lymphocytes. The cut-off value, established in nuclei from the apparently tumor-free contralateral thyroid lobe was calculated as the beta inverse function and was split FISH signals in 2.4% of cells for *RET* and 0% for *PPAR γ* . Probe efficiency was confirmed on nuclei from PTCs and FTCs positive for *RET/PTC* and *PAX8/PPAR γ* alterations by conventional RT-PCR. On this basis, we studied from 150 to 200 nuclei *per* sample and considered a sample positive if a broken signal for *RET* or *PPAR γ* was observed in $\geq 3\%$ of nuclei.³²

3 | RESULTS

3.1 | Low presence of RET and absence of PPAR γ rearrangements in the study cohort

Somatic mutations in thyroid tumors such as RET/PTC and PAX8/PPAR γ chromosomal rearrangements are frequently used in clinical mutation panels to detect malignant thyroid cancers. Among 60 cases analyzed, a split-apart RET FISH signal was identified in 2 (3.3%) samples (one CPTC and one NIFTP), the percentage of positive nuclei was 38% (57/150) and 24% (36/150). No PPAR γ rearrangements were found in our cohort (Figure 1A,B). In addition, we did not observe alterations in the NAT.

3.2 | NIFTP has a higher frequency of long telomeres than CPTC and FVPTC

We investigated the 3D telomere profiles of three histotypes to determine whether or not we could detect thyroid histotype-specific profiles. We analyzed 60 paraffin embedded tissues of thyroid nodules, 20 CPTC, 20 FVPTC and 20 NIFTP and normal tissue adjacent to the tumors (NAT). Five of six TeloView telomeric parameters (number of telomeric signals, number of telomere aggregates, average intensity, total intensity and nuclear volume) differentiated NAT from tumor tissues (Table 2).

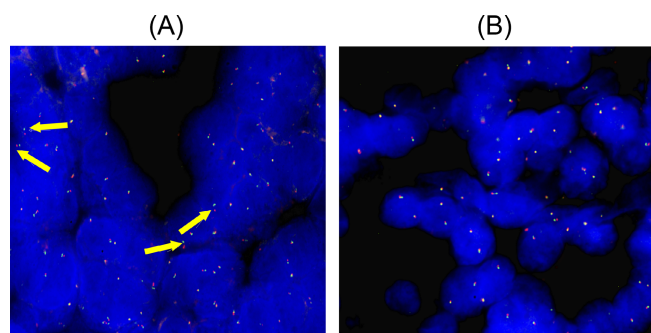


FIGURE 1 I-FISH with break-apart DNA probes specific for RET and PPAR γ genes. (A) Yellow arrows show the split of one red/green signal indicating disruption of RET gene copy. (B) Example of nuclei with two red/green fused signals indicates PPAR γ gene integrity.

TABLE 2 Statistical analysis of 3D telomere parameters of thyroid tumor vs normal to adjacent tumor tissue.

Histotype	Number of telomere signals	Number of telomere aggregates	Average intensity	Total intensity	a/c ratio	Nuclear Volume
NIFTP	$P < .0001$ (\downarrow NTA vs T \uparrow)	$P < .001$ (\downarrow NTA vs T \uparrow)	$P < .001$ (\uparrow NTA vs T \downarrow)	$P < .001$ (\uparrow NTA vs T \downarrow)	ns	$P < .001$ (\downarrow NTA vs T \uparrow)
CPTC	$P < .0001$ (\downarrow NTA vs T \uparrow)	$P < .001$ (\downarrow NTA vs T \uparrow)	$P < .001$ (\uparrow NTA vs T \downarrow)	$P < .001$ (\uparrow NTA vs T \downarrow)	ns	$P < .001$ (\downarrow NTA vs T \uparrow)
FVPTC	$P < .0001$ (\downarrow NTA vs T \uparrow)	$P < .001$ (\downarrow NTA vs T \uparrow)	$P < .001$ (\uparrow NTA vs T \downarrow)	$P < .001$ (\uparrow NTA vs T \downarrow)	ns	$P < .001$ (\downarrow NTA vs T \uparrow)

Abbreviations: CPTC, classic thyroid papillary carcinoma; FVPTC, follicular variant of papillary thyroid carcinoma; NAT, normal adjacent tissue; NIFTP, noninvasive follicular thyroid neoplasm with papillary-like nuclear features; T, tumor; \downarrow , decrease; \uparrow , increase; ns, not significant.

NIFTP could be differentiated from CPTC and FVPTC by analysis of telomere signal intensities, subdivided into four quartiles (Figure 2). Relative telomere signal intensities measured in arbitrary units (a.u.) represent telomere length.³³ Four cell subpopulations (quartiles) were examined, based on their telomeric signal intensities in arbitrary units (a.u.): cells with very short telomeres (≤ 5000 a.u.), cells with short telomeres (5001-9000 a.u.), cell with medium telomeres (9001-16 000 a.u.) and cells with large telomeres (>16.000 a.u.). As shown in Figure 2, NIFTP had significantly more cells with long telomeres (>16.000 a.u.) than the other histotypes. Significant differences were also found in the short (5001-9000 a.u.) and medium sized (9001-16 000 a.u.) telomere quartiles. However, no significant difference was observed in the frequency distribution of very short telomeres (≤ 5000 a.u.). We conclude that NIFTP cases present with longer telomeres than either CPTC or FVPTC.

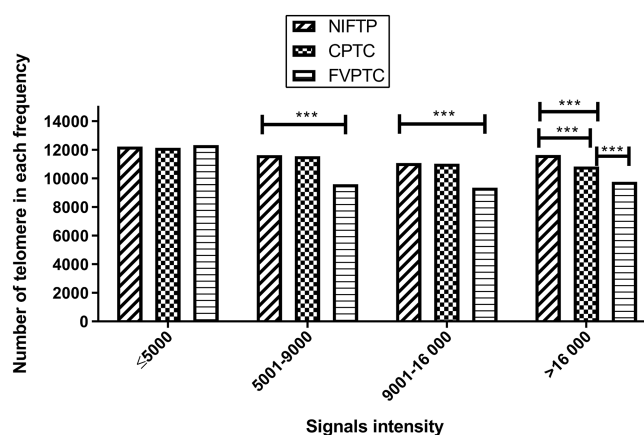


FIGURE 2 Bar plot of the differences among telomeric signal intensity (telomere length) differences in quartiles between CPTC, FVPTC and NIFTP. Nuclei with intensities of >16.000 a.u. represent very large telomeres. In the quartile analysis, <5000 a.u. represent very short, 5001 to 9000 a.u. short, 9001 to 16 000 a.u. medium-sized telomeres, respectively. The x-axis assigns one box for each cell population analyzed. The y-axis refers to the number of telomeres in different quartiles. We only show P values, $*** P < .0001$. CPTC, classic thyroid papillary carcinoma; FVPTC, follicular variant of papillary thyroid carcinoma; NIFTP, noninvasive follicular thyroid neoplasm with papillary-like nuclear features. Representative figures of the telomere staining are shown in Figure S1. A different representation of the same data is shown in Figure S2.

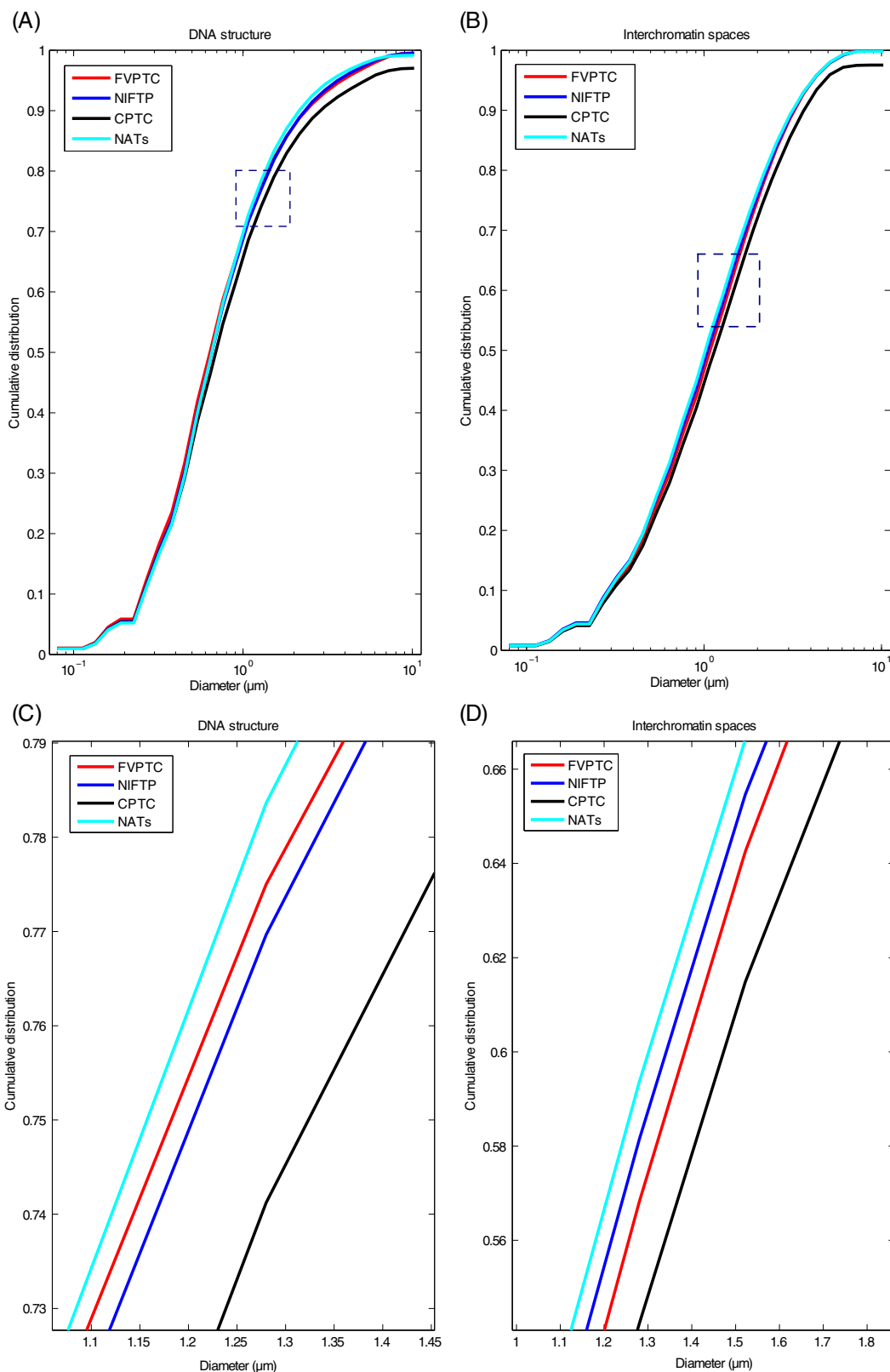


FIGURE 3 Three-dimensional (3D)-structured illumination microscopy (SIM) identify significant differences in DNA structure between normal adjacent tissue (NATs), noninvasive follicular thyroid neoplasm with papillary-like nuclear features (NIFTP), classic papillary thyroid carcinoma (CPTC), follicular variant of papillary thyroid carcinoma (FVPTC). (A) Cumulative distribution and diameter of DNA structure between PTC histotypes; (B) cumulative distribution and diameter of interchromatin spaces between PTC histotypes; (C,D) are enlarged versions from the boxes above. Figure S3 illustrates representative 3D-SIM images for DNA structure and interchromatin spaces.

3.3 | Chromatin de-condensation is a nuclear marker of PTC histotypes and could be used as a differential feature to exclude NIFTP

Super-resolution imaging of the genome provides high-resolution information about chromatin organization. Granulometry

TABLE 3 Statistical analysis and *P*-values for the comparisons in Figure 3A,B.

Group 1	Group 2	<i>P</i> -value
<i>2-2-KS-test for light granulometries (DNA structure)</i>		
NATs	FVPTC	<.0001
NATs	NIFTP	.000260638
NATs	CPTC	<.0001
FVPTC	NIFTP	<.0001
FVPTC	CPTC	<.0001
NIFTP	CPTC	<.0001
<i>2-2-KS-test for dark granulometries (Interchromatin spaces)</i>		
NATs	FVPTC	<.0001
NATs	NIFTP	.503796688
NATs	CPTC	<.0001
FVPTC	NIFTP	.000315958
FVPTC	CPTC	<.0001
NIFTP	CPTC	<.0001

quantitatively assesses the DNA size distribution and the differences in the DNA structure and interchromatin spaces in normal and cancer cells.¹⁸ To determine whether chromatin organization patterns allow for differentiation of thyroid cancer histotypes, we imaged and quantified pathological tissue (CPTC, FVPTC and NIFTP) and compared it to the corresponding normal adjacent tissue (NAT) for each different histotype. Using granulometry, we measured DNA granule sizes detected in the 3D-SIM images as well as the DNA-free spaces, which represent interchromatin spaces. Super-resolution imaging revealed significant differences in DNA decompaction among PTC histotypes. NATs samples have more densely packaged DNA followed by NIFTP, FVPTC and CPTC with high overall DNA de-condensation (Figure 3A,C). Interestingly, the same pattern was observed for the size of the interchromatin spaces: the interchromatin spaces increase starting from NAT/NIFTP followed by FVPTC and CPTC, with the largest interchromatin spaces in CPTC (Figure 3B,D). There are no significant differences between NATs and NIFTP in relation to interchromatin spaces (Figure 3D [two blue lines] and Table 3).

Next, due to the observed heterogeneous patterns in NIFTP described by Macerola et al.,³⁴ we used 3D-SIM to compare the measurements of individual NIFTP tissues within the group (Figure S4). As presented in Figure 4, the NATs measurements of DNA structure (light-blue line) clearly separate the NIFTP samples into two groups with more and less condensed chromatin (Figure 4A). The same is observed with the size of interchromatin spaces (Figure 4B).

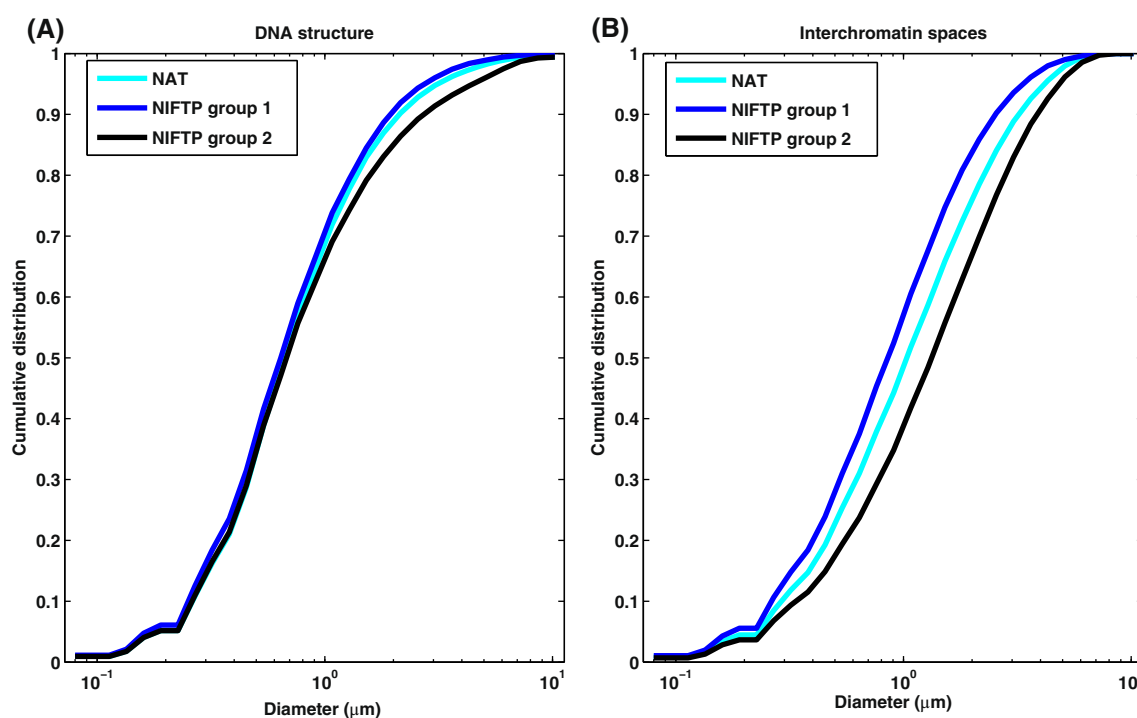


FIGURE 4 The 3D-SIM identifies two subgroups within noninvasive follicular thyroid neoplasm with papillary-like nuclear features (NIFTP) group. The two groups are compared to normal adjacent tissue (NATs). (A) Cumulative distribution and diameter of DNA structure. (B) Cumulative distribution and diameters of interchromatin spaces.

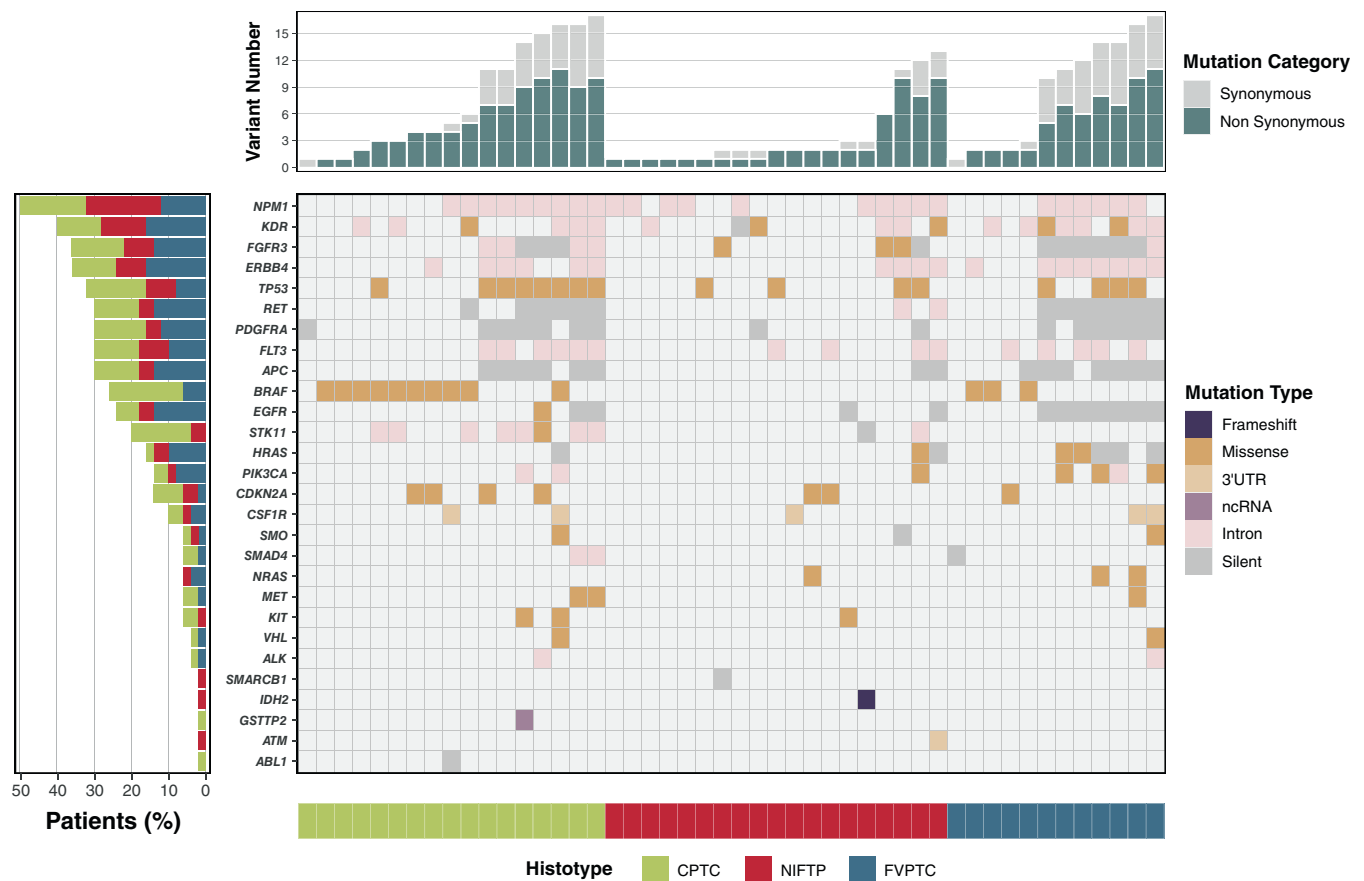


FIGURE 5 Summary of all somatic variants found in patients with thyroid cancer. CoMut Plot summarizing the main findings from the onco-panel regarding the mutational profile analysis. (Center panel) Plot showing all types of somatic mutations (shown with different colors) found for 28 protein-coding genes (sorted by number of alterations—see left graph) in our cohort of 48 samples (sorted by their respective histotypes—see bottom graph—and, within each histotype, by variant number—see top graph). Unfilled boxes indicate the absence of alteration for a given set of gene/sample; (Bottom panel) bar indicating with different colors the histotype of the samples; (Top panel) Bar plot showing the total (synonymous and nonsynonymous) number of somatic variations for all samples, also ordered by histotype and, within each histotype, by number of variations; (Left panel) Horizontal bar plot showing the percentage of patients (each color represents their corresponding histotypes) containing somatic alterations in the genes shown, ordered from the most mutated to the least mutated. The complete list of variants and specific changes for all patients are described in Table S4. 3'UTR, 3 prime untranslated region; CPTC, classical papillary thyroid carcinoma; FVPTC, follicular variant of papillary thyroid carcinoma; ncRNA, noncoding RNA; NIFTP, noninvasive follicular thyroid neoplasm with papillary-like nuclear features.

3.4 | NIFTP, FVPTC and PTC have specific mutational profiles

DNA extracted from tumor specimens and their respective normal adjacent tissues resulted in sufficient DNA amount and quality for downstream sequencing-analysis of 48 samples (CPTC = 17; FVPTC = 12; NIFTP = 19). Over 48 genes analyzed, we found alterations in 28 hotspot genes (Figure 5). The list of genes investigated, and targeted sequencing area is shown in Tables S1 to S3. Using matched adjacent normal tissue, we distinguish between germline and somatic variations. SNVs or INDELs found in the NAT for each tumor were considered as germline and were excluded from the analysis. Figure 5 shows the results for all 48 patients analyzed, variation burden, altered genes and mutation type observed. Sixty percent (60%) (10 out of the 17 samples) of

the CPTC samples harbored a *BRAF*^{V600E} mutations. We observed *NRAS* mutations in one NIFTP case (1 out of 19, 5.2%). As expected, NIFTP was characterized by the lack of *BRAF*^{V600E} mutation (Figure 5). In addition, tumor variation burden, which indicates the number of mutations seen in a section of DNA per mega base, was lower in NIFTP cases compared to CPTC and FVPTC.

4 | DISCUSSION

It has long been recognized and accepted that histopathology is the “gold standard” for treatment decisions and evaluation of outcomes for thyroid neoplasms. However, there is considerable diagnostic variability among pathologists when examining follicular-patterned thyroid nodules.³⁵ This particularly evident in

follicular lesions where both benign and malignant lesions have similar architectural features,²¹ which leads to increasing diagnostic complexity. This aspect is even more challenging in accurately differentiating the recently recognized “non-invasive follicular thyroid neoplasm with papillary-like nuclear features” (NIFTP) from CPTC and FVPTC and its classification as a benign lesion. Outcome studies in patients with NIFTP have reported lymph node metastases in some patients.³⁶ Therefore, the classification of this entity as a truly benign lesion continues to be controversial. To address this problem, molecular markers are being used to help delineate benign from malignant thyroid lesions, differentiate the various follicular neoplasms and provide potential prognostic biomarkers for treatment decisions.³⁷ The large-scale study of The Cancer Genome Atlas (TCGA) identified a 71-gene signature that divided PTCs into *BRAF*^{V600E}-like and *RAS*-like tumors.³⁸ Although molecular profile analyses of NIFTP are limited, being considered helpful but not required for the diagnosis, there is an indication that they typically enter the *RAS*-like group.³⁹ This molecular approach is useful in most, but not all cases of NIFTP. This has been well documented in outcome studies in which patients with NIFTP have reported lymph node metastases in some nodules, which apparently met the stringent NIFTP classification criteria.⁴⁰

To overcome these limitations and add knowledge to NIFTP biology we have explored the potential of a single-cell approach to refine the diagnosis of this entity. Single-cell techniques, including telomere pattern analysis, have been shown to be a powerful tool for deciphering the cellular and molecular landscapes in cancers and elucidating cancer lesions' biological characteristics and dynamics.¹⁰ Telomere dysfunction is considered the primary mechanism for cancer survival and aggressiveness.⁴¹ The progressive telomere shortening is a rate-limiting step for uncontrolled cell proliferation.³⁷ As with other groups, we have reported a significantly higher frequency of short telomeres in thyroid cancers compared to normal thyroid tissue.⁴² However, in the present study, the various histotypes did not show significant differences in the number of short telomeres and other telomere features, preventing the use of these variables to differentiate nodules. In contrast and remarkably, the number of long telomeres was significantly different among histotypes, with NIFTP having the highest frequency of long telomeres (>16,000 a.u.) followed by CPTC and FVPTC (Figure 2). This was an encouraging result, indicating that this single cell approach could be used as a biomarker to distinguish NIFTP from CPTC and FVPTC.

The development of new microscopes and cutting-edge imaging-based methods, including three-dimensional and super-resolution microscopy has a crucial role in understanding chromatin and nuclear architecture. It has been suggested that the nuclear localization of genes might be dynamically regulated relative to their expression⁴³ and that, while active nuclear compartment has lower DNA density and active gene transcription, the inactive nuclear compartment has a high DNA density.⁴⁴ Indeed, cancer cells can reprogram the chromatin status to increase chromatin accessibility by transcription factors and DNA repair machinery during damage.⁴⁵ In this context, our 3D-SIM data highlight statistically significant differences in the DNA structure

and interchromatin spaces among the thyroid cancer histotypes. A striking progression of DNA de-condensation was detected across histotypes, with the consistent progression of DNA de-condensation from more densely packaged DNA in normal thyroid tissue followed by NIFTP, FVPTC and CPTC (with overall high de-condensation of DNA). A similar trend was observed for the size of interchromatin spaces, which increased starting from NAT/NIFTP followed by FVPTC and CPTC (with the largest interchromatin spaces) (Figure 3). It seems that thyroid cells develop ways to impair heterochromatin structure during malignant transformation, which could trigger important signaling cascades that lead to tumorigenesis. Indeed, the presence of an aberrant 3D genome (high overall DNA de-condensation and increase of interchromatin spaces) in PTC and FVPTC tumors compared to normal tissue and NIFTP could lead to promoting tumor cell aggressiveness. The clearcut 3D-SIM distinction between the thyroid subtypes, coupled with the above-mentioned observation that NIFTP has the highest frequency of long telomeres, may be used as a differentiating characteristic of NIFTP. To support the hypothesis that 3D chromatin architecture could be used to grade NIFTP lesions, we have used the grading information (unifocal vs multifocal) to show insights the potential of this parameter for thyroid lesions (Figures S5 and S6). However, due to the sample size, the prognostic significance and the biological importance of these findings deserve further studies.

The existing molecular panel for thyroid nodules is inconclusive, where the same markers are also prevalent in benign thyroid nodules. Up to 48% of benign thyroid lesions have *RAS* mutations, up to 68% have *RET/PTC* rearrangements and up to 55% of benign thyroid lesions have *PAX/PPAR γ* rearrangements.⁵⁴ Although, the prevalence of these markers is significantly higher in malignant lesions, relying upon their presence for differential diagnosis and clinical decision making for an indeterminate thyroid lesion might result in misclassification or overtreatment of potentially benign lesions. In our cohort, FISH analysis showed *RET/PTC* rearrangements in a few patients (3.3%) and *PPAR γ* rearrangements in none of the patients. The prevalence of *RET* rearrangements in sporadic PTC is highly heterogeneous (ranging from 2.5% to 73%), due to ethnicity, different geographical location, environmental exposure and the method used for their identification and genetic heterogeneity.⁴⁶ *PPAR γ* rearrangements, which may be detected in typical follicular thyroid carcinoma (FTC), FVPTC, NIFTP and only in 0% to 1% of PTC were missing in our cohort (Figure 1), possibly due to the small number of cases.

The further molecular characterization of the samples through a custom-designed onco-panel showed a consistent presence of *BRAF*^{V600E} in PTC and FVPTC, and its absence in NIFTP. The lack of *BRAF*^{V600E} is a relevant secondary diagnostic criteria⁴⁷ of NIFTP. However, as shown in Figure 5, *TP53* variations were found in four NIFTP. The most frequent was *TP53* rs1042522 (Arg72Pro). This finding prompted us to conduct a pathological review of nodules carrying *TP53* variants since the presence of *TP53* mutations is a secondary exclusion criterion of the NIFTP classification.⁴⁷ The revision still met the revised NIFTP primary histological criteria,⁴⁷ including encapsulation or clear demarcation from adjacent thyroid parenchyma, follicular growth pattern without well-formed papillae, absence of

psammoma bodies and solid growth pattern <30%/trabecular/ insular. The confirmed diagnosis is in line with ongoing evidence that *TP53* coding region variants are far more prevalent than previously suspected. Hence, attention must be paid to “Finding the needles in a haystack of pathogenic variants.”⁴⁸ Evidence has been accumulated indicating that *TP53* variants may have implications other than in tumor suppression function. The arg allele of rs1042522 is slightly more active in inducing apoptosis⁴⁹ and it has been associated with winter temperature. Indeed, this variant is considered benign in the ClinVar archive according to the American College of Medical Genetics and Genomics (ACMG) criteria, and recently the effect of *TP53*-rs1042522 variants on decreased risk of PTC, smaller tumor size and lower incidence of vascular invasion was described.⁵⁰ Nevertheless, we observed that NIFTP nodules with these variants had significant differences in chromatin condensation ($P = .0002$). Further study of cases with the same variant will clarify if this association may characterize a subtype of NIFTPs.

An important finding from the onco-panel is a low variation burden, defined as the number of somatic variations per mega base, found in NIFTP samples. However, due to differences in panel size, mutation types and bioinformatic platforms analysis, tumor burden analysis used as a predictive biomarker is not clear and requires further study.

Altogether our results indicate that, compared to the molecular approach, the single-cell approach achieved by the 3D-SIM examination has a much greater potential in identifying NIFTP-specific features (Figures 4 and S4). The NIFTP groups presented in Figure 4 do not show significant differences in telomere structure and/or number of SNVs. However, the prognostic significance of these features and their biological behavior clearly deserve additional further study.

In summary, this is the first study to investigate the 3D structural organization of the genome to differentiate papillary and follicular thyroid cancer subtypes. Our data indicate that NIFTP has a specific 3D genome organization similar to normal thyroid tissue and that it is clearly different from that of classical and follicular variant PTC. These results, while reinforcing the idea that NIFTP is a lesion with a low risk of disease progression, underscore the existence of heterogeneity within the group (Figure 4). We will continue to explore this in a long-term follow-up study, confident that this innovative approach could also be applied to fine needle aspirates in the initial diagnosis of thyroid malignancy.

5 | CONCLUSIONS

NIFTP requires additional precise and innovative markers in clinical practice. The differentiation of NIFTP from CPTC and FVPTC by onco-panel sequencing in our limited cohort did not yield useful molecular information that might be applied clinically. The 3D structural architecture of the genome revealed by super resolution imaging of nuclear DNA organization and 3D imaging of telomeres allowed for the robust and reliable differentiation of NIFTP from CPTC and

FVPTC and distinguished all the histotypes from normal adjacent thyroid tissues. We conclude that the structural organization of the genome provides additional key data for each thyroid cancer subtype to enable its distinction from other morphologically similar thyroid cancer histotypes.

AUTHOR CONTRIBUTIONS

Aline Rangel-Pozzo: Conceptualization; Data Curation; Formal Analysis; Investigation; Project Administration; Software; Visualization; Writing – original draft; Writing – review & editing. **Filipe F. dos Santos:** Data Curation; Formal Analysis; Software; Visualization; Writing – review & editing. **Tinuccia Dettori:** Investigation; Writing – review & editing. **Matteo Giulietti:** Formal Analysis; Investigation; Writing – review & editing. **Daniela Virginia Frau:** Investigation; Writing – review & editing. **Pedro A. F. Galante:** Conceptualization; Software; Supervision; Visualization; Writing – review & editing. **Roberta Vanni:** Conceptualization; Supervision; Visualization; Writing – review & editing. **Alok Pathak:** Investigation; Writing – review & editing. **Gabor Fischer:** Investigation; Writing – review & editing. **John Gartner:** Conceptualization; Investigation; Writing – review & editing. **Paola Caria:** Conceptualization; Data Curation; Investigation; Methodology; Project Administration; Resources; Supervision; Visualization; Writing – original draft; Writing – review & editing. **Sabine Mai:** Conceptualization; Funding Acquisition; Methodology; Project Administration; Resources; Supervision; Visualization; Writing – review & editing. All authors have read and agreed to the published version of the article. The work reported in the article has been performed by the authors, unless clearly specified in the text.

ACKNOWLEDGEMENTS

Imaging was performed at the Genomic Centre for Cancer Research and Diagnosis, a Canada Foundation for Innovation-funded facility. The authors thank the Rady Innovation Fund for support of this work and Canada Research Chair (Tier 1) funding to SM as well as FAPESP scholarship support 2020/14158-9 for FFdS. We acknowledge the CeSAR (Centro Servizi Ricerca d'Ateneo) core facility of the University of Cagliari and Marta Costa for assistance with the generation of the sequencing data. We thank Mary Cheang for statistical analyses.

FUNDING INFORMATION

This project was funded by the Rady Innovation Fund.

CONFLICT OF INTEREST STATEMENT

Dr. Sabine Mai co-founded Telo Genomics Corp (Toronto, ON, Canada). She is a director, shareholder and Chair of the Clinical and Scientific Advisory Board. The other authors declare no conflict of interest.

DATA AVAILABILITY STATEMENT

The sequencing experiment produced raw FASTQ files (sequencing data available at ENA database, <https://www.ebi.ac.uk/ena/browser/home>, ENA accession: PRJEB52871). The data that support the findings of our study are available from the corresponding author upon reasonable request.

ETHICS STATEMENT

Our study was conducted in accordance with the institutional review board approval of the Health Research Ethics Board on human studies from University of Manitoba, Canada (Ethic number: HS21723; H2018:156).

ORCID

Sabine Mai  <https://orcid.org/0000-0002-5797-2201>

REFERENCES

- Davies L, Welch HG. Increasing incidence of thyroid cancer in the United States, 1973-2002. *JAMA*. 2006;295:2164-2167.
- LiVolsi VA. Papillary thyroid carcinoma: an update. *Mod Pathol*. 2011;24(Suppl 2):S1-S9.
- Chen KTK, Rosai J. Follicular variant of thyroid papillary carcinoma: a clinicopathologic study of six cases. *Am J Surg Pathol*. 1977;1:123-130.
- Nikiforov YE, Seethala RR, Tallini G, et al. Nomenclature revision for encapsulated follicular variant of papillary thyroid carcinoma: a paradigm shift to reduce overtreatment of indolent tumors. *JAMA Oncol*. 2016;2:1023-1029.
- Kholová I, Haaga E, Ludvik J, Kalfert D, Ludvikova M. Noninvasive follicular thyroid neoplasm with papillary-like nuclear features (NIFTP): tumour entity with a short history. A review on challenges in our microscopes, molecular and ultrasonographic profile. *Diagnosics*. 2022;12:250.
- Chu Y-H, Sadow PM. Noninvasive follicular thyroid neoplasm with papillary-like nuclear features (NIFTP): diagnostic updates and molecular advances. *Semin Diagn Pathol*. 2020;37:213-218.
- Zajkowska K, Kopczyński J, Gózdź S, Kowalska A. Noninvasive follicular thyroid neoplasm with papillary-like nuclear features: a problematic entity. *Endocr Connect*. 2020;9:R47-R58.
- Alves VAF, Kakudo K, LiVolsi V, et al. Noninvasive follicular thyroid neoplasm with papillary-like nuclear features (NIFTP): achieving better agreement by refining diagnostic criteria. *Clinics*. 2018;73:e576.
- Vermolen BJ, Garini Y, Mai S, et al. Characterizing the three-dimensional organization of telomeres. *Cytometry*. 2005;67A:144-150.
- Babu D, Fullwood MJ. 3D genome organization in health and disease: emerging opportunities in cancer translational medicine. *Nucleus*. 2015;6:382-393.
- Gadji M, Adebayo Awe J, Rodrigues P, et al. Profiling three-dimensional nuclear telomeric architecture of myelodysplastic syndromes and acute myeloid leukemia defines patient subgroups. *Clin Cancer Res*. 2012;18:3293-3304.
- Gadji M, Fortin D, Tsanaclis A-M, et al. Three-dimensional nuclear telomere architecture is associated with differential time to progression and overall survival in glioblastoma patients. *Neoplasia*. 2010;12:183-191.
- Knecht H, Kongruttanachok N, Sawan B, et al. Three-dimensional telomere signatures of Hodgkin- and reed-Sternberg cells at diagnosis identify patients with poor response to conventional chemotherapy. *Transl Oncol*. 2012;5:269-277.
- Kuzyk A, Gartner J, Mai S. Identification of neuroblastoma subgroups based on three-dimensional telomere organization. *Transl Oncol*. 2016;9:348-356.
- Drachenberg D, Awe J, Rangel Pozzo A, Saranchuk J, Mai S. Advancing risk assessment of intermediate risk prostate cancer patients. *Cancer*. 2019;11:855.
- Rangel-Pozzo A, Yu P, LaL S, et al. Telomere architecture correlates with aggressiveness in multiple myeloma. *Cancer*. 2021;13:1969.
- Rangel-Pozzo A, Kuzyk A, Gartner J, Mai S. MYCN overexpression is linked to significant differences in nuclear DNA organization in neuroblastoma. *Biomed J*. 2019;63:3.
- Righolt CH, Guffei A, Knecht H, et al. Differences in nuclear DNA organization between lymphocytes, Hodgkin and reed-Sternberg cells revealed by structured illumination microscopy. *J Cell Biochem*. 2014;115:1441-1448.
- Righolt CH, Knecht H, Mai S. DNA superresolution structure of Reed-Sternberg cells differs between long-lasting remission versus relapsing Hodgkin's lymphoma patients: DNA structure in pre-treatment Hodgkin's lymphoma. *J Cell Biochem*. 2016;117:1633-1637.
- Sathitruangsak C, Righolt CH, Klewes L, et al. Quantitative superresolution microscopy reveals differences in nuclear DNA organization of multiple myeloma and monoclonal gammopathy of undetermined significance. *J Cell Biochem*. 2015;116:704-710.
- Madsen MB, Kiss K, Cilius Nielsen F, Bennedbak FN, Rossing M. Amplicon-based NGS panels for actionable cancer target identification in follicular cell-derived thyroid neoplasia. *Front Endocrinol (Lausanne)*. 2020;11:146.
- Osamura RY, Klöppel G, Rosai JLR. *WHO Classification of Tumours of Endocrine Organs*. 4th ed. Lyon, France: IARC; 2017.
- Schaefer LH, Schuster D, Herz H. Generalized approach for accelerated maximum likelihood based image restoration applied to three-dimensional fluorescence microscopy: accelerated ML image restoration approach. *J Microsc*. 2002;204:99-107.
- <https://emea.illumina.com/systems/sequencing-platforms.html>
- <https://www.bioinformatics.babraham.ac.uk/projects/fastqc/>
- Bolger AM, Lohse M, Usadel B. Trimmomatic: a flexible trimmer for Illumina sequence data. *Bioinformatics*. 2014;30:2114-2120.
- Li H, Durbin R. Fast and accurate long-read alignment with burrows-Wheeler transform. *Bioinformatics*. 2010;26:589-595.
- Danecek P, Bonfield JK, Liddle J, et al. Twelve years of SAMtools and BCFtools. *Gigascience*. 2021;10:giab008.
- van der Auwera BD, O'Connor GA. *Genomics in the Cloud*. Sebastopol, CA: O'Reilly Media, Inc.; 2020.
- Wang K, Li M, Hakonarson H. ANNOVAR: functional annotation of genetic variants from high-throughput sequencing data. *Nucleic Acids Res*. 2010;38:e164.
- Fred L, Drake GVR. *Python 3 Reference Manual*. Scotts Valley, CA: CreateSpace Independent Publishing Platform; 2009.
- Caria P, Frau DV, Dettori T, et al. Optimizing detection of RET and PPARγ rearrangements in thyroid neoplastic cells using a home-brew tetracolor probe. *Cancer Cytopathol*. 2014;122:377-385.
- Poon SS, Martens UM, Ward RK, Lansdorp PM. Telomere length measurements using digital fluorescence microscopy. *Cytometry*. 1999;36:267-278.
- Macerola E, Proietti A, Basolo F. Noninvasive follicular neoplasm with papillary-like nuclear features (NIFTP): a new entity. *Gland Surg*. 2020;9:S47-S53.
- Liu H, Lin F. Application of immunohistochemistry in thyroid pathology. *Arch Pathol Lab Med*. 2015;139:67-82.
- Rosario PW, Mourão GF. Noninvasive follicular thyroid neoplasm with papillary-like nuclear features (NIFTP): a review for clinicians. *Endocr Relat Cancer*. 2019;26:R259-R266.
- Rangel-Pozzo A, Sisdelli L, Cordioli MIV, et al. Genetic landscape of papillary thyroid carcinoma and nuclear architecture: an overview comparing pediatric and adult populations. *Cancers (Basel)*. 2020;12:E3146.
- Agrawal N, Akbani R, Aksoy BA, et al. Integrated genomic characterization of papillary thyroid carcinoma. *Cell*. 2014;159:676-690.
- Brandler TC, Liu CZ, Cho M, et al. Does noninvasive follicular thyroid neoplasm with papillary-like nuclear features (NIFTP) have a unique molecular profile? *Am J Clin Pathol*. 2018;150:451-460.

40. Cho U, Mete O, Kim M-H, Bae JS, Jung CK. Molecular correlates and rate of lymph node metastasis of non-invasive follicular thyroid neoplasm with papillary-like nuclear features and invasive follicular variant papillary thyroid carcinoma: the impact of rigid criteria to distinguish non-invasive follicular thyroid neoplasm with papillary-like nuclear features. *Mod Pathol*. 2017;30:810-825.
41. Donati B, Ciarrocchi A. Telomerase and telomeres biology in thyroid cancer. *IJMS*. 2019;20:2887.
42. Rangel-Pozzo A, Dettori T, Virginia Frau D, et al. Three-dimensional telomere profiles in papillary thyroid cancer variants: a pilot study. *Bosn J Basic Med Sci*. 2021;22:481-487.
43. Meldi L, Brickner JH. Compartmentalization of the nucleus. *Trends Cell Biol*. 2011;21:701-708.
44. Cremer T, Cremer M, Hübner B, et al. The 4D nucleome: evidence for a dynamic nuclear landscape based on co-aligned active and inactive nuclear compartments. *FEBS Lett*. 2015;589:2931-2943.
45. Yu S, Yang F, Shen WH. Genome maintenance in the context of 4D chromatin condensation. *Cell Mol Life Sci*. 2016;73:3137-3150.
46. Li AY, McCusker MG, Russo A, et al. RET fusions in solid tumors. *Cancer Treat Rev*. 2019;81:101911.
47. Nikiforov YE, Baloch ZW, Hodak SP, et al. Change in diagnostic criteria for noninvasive follicular thyroid neoplasm with papillary-like nuclear features. *JAMA Oncol*. 2018;4:1125-1126.
48. Soussi T. Benign SNPs in the coding region of *TP53*: finding the needles in a haystack of pathogenic variants. *Cancer Res*. 2022;82:3420-3431.
49. Murphy ME. Polymorphic variants in the p53 pathway. *Cell Death Differ*. 2006;13:916-920.
50. Heidari Z, Harati-Sadegh M, Arian A, Maruei-Milan R, Salimi S. The effect of *TP53* and *P21* gene polymorphisms on papillary thyroid carcinoma susceptibility and clinical/pathological features. *IUBMB Life*. 2020;72:922-930.

SUPPORTING INFORMATION

Additional supporting information can be found online in the Supporting Information section at the end of this article.

How to cite this article: Rangel-Pozzo A, dos Santos FF, Dettori T, et al. Three-dimensional nuclear architecture distinguishes thyroid cancer histotypes. *Int J Cancer*. 2023; 153(10):1842-1853. doi:[10.1002/ijc.34667](https://doi.org/10.1002/ijc.34667)